Metallofullerene and fullerene formation from condensing carbon gas under conditions of stellar outflows and implication to stardust

Paul W. Dunk[a,b,1], Jean-Joseph Adjizian[c], Nathan K. Kaiser[b], John P. Quinn[b], Gregory T. Blakney[b], Christopher P. Ewels[c,1], Alan G. Marshall[a,b,1], and Harold W. Kroto[a,1]

[a]Department of Chemistry and Biochemistry, Florida State University, Tallahassee, FL 32306; [b]Ion Cyclotron Resonance Program, National High Magnetic Field Laboratory, Florida State University, Tallahassee, FL 32310; and [c]Institut des Matériaux Jean Rouxel, Centre National de la Recherche Scientifique, Unité Mixte de Recherche 6502, Université de Nantes, BP 32229 Nantes, France

Contributed by Harold W. Kroto, August 29, 2013 (sent for review June 13, 2013)

Carbonaceous presolar grains of supernovae origin have long been isolated and are determined to be the carrier of anomalous ^{22}Ne in ancient meteorites. That exotic ^{22}Ne is, in fact, the decay isotope of relatively short-lived ^{22}Na formed by explosive nucleosynthesis, and therefore, a selective and rapid Na physical trapping mechanism must take place during carbon condensation in supernova ejecta. Elucidation of the processes that trap Na and produce large carbon molecules should yield insight into carbon stardust enrichment and formation. Herein, we demonstrate that Na effectively nucleates formation of Na@C_{60} and other metallofullerenes during carbon condensation under highly energetic conditions in oxygen- and hydrogen-rich environments. Thus, fundamental carbon chemistry that leads to trapping of Na is revealed, and should be directly applicable to gas-phase chemistry involving stellar environments, such as supernova ejecta. The results indicate that, in addition to empty fullerenes, metallofullerenes should be constituents of stellar/circumstellar and interstellar space. In addition, gas-phase reactions of fullerenes with polycyclic aromatic hydrocarbons are investigated to probe "build-up" and formation of carbon stardust, and provide insight into fullerene astrochemistry.

One of the most profound findings in cosmochemistry has been the isolation and study of presolar grains recovered from carbonaceous chondrites, which are ancient meteorites (1–3). A particularly striking example is the micrometer-sized low-density graphite grains of supernovae origin (1, 4). This discovery was due to identification of noble gas isotopic anomalies identified by mass spectrometry; upon stepwise heating of bulk samples of carbonaceous chondrite, highly enriched ^{22}Ne is released (3, 4). That observation led to the possibility that exotic ^{22}Ne was a decay product of the extinct nuclide ^{22}Na, produced from a supernova explosion (5). Subsequently, ^{22}Ne was used as a guide to pinpoint the tiny carbonaceous grains embedded within the bulk meteorite, and the supernovae origin was further confirmed by other isotopic "cosmic fingerprints" (2–4). Thus, these particular carbonaceous grains represent a direct chemical sample from a supernova.

Despite many detailed experiments on presolar carbonaceous grains, the mechanism whereby ^{22}Na is selectively trapped to enrich stardust remains a puzzle. The carbon chemistry of supernova ejecta, in part, determines the composition of carbon stardust. Supernovae-originating dust is ejected into the interstellar medium (ISM), directly impacting interstellar chemistry and subsequent stellar evolution. Furthermore, dust is ubiquitous in the universe, and recent observational studies suggest that supernovae are major dust contributors (6–8). Therefore, study of the gas-phase chemical processes that can operate under conditions of stellar outflows should provide insight into a broad range of phenomena, including stellar and interstellar chemistry, distribution of carbon in the universe, and supernova mixing.

Fullerenes have been principal astronomic molecular targets since the discovery of Buckminsterfullerene, C_{60} (9, 10). The closed-caged molecules, however, have only recently been confirmed to exist in circumstellar and interstellar environments. C_{60} and C_{70} were first unequivocally detected in a planetary nebula in 2010, which was thought to be hydrogen deficient (11). Thereafter, Buckminsterfullerene was detected in hydrogen-rich [including the least H-deficient R Coronae Borealis stars] (12, 13) and oxygen-rich environments (14), as well as the ISM (15) and a protoplanetary nebula (16). Moreover, fullerenes have been detected in a host of other circumstellar and interstellar sources, with new reports of cosmic fullerene detection constantly emerging.

Fullerenes have recently been experimentally shown to self-assemble in condensing carbon through a closed network growth (CNG) mechanism (17, 18), in which small fullerenes form initially and then progress into larger species, such as C_{60}, by incorporation of atomic and diatomic carbon into growing cages. That process resolves how fullerenes form spontaneously under highly energetic conditions from carbon vapor, as well as how C_{60} forms as the most abundant species. The CNG mechanism for fullerene formation should occur in condensing carbon vapor of stellar ejecta; although, formation by photochemical processing of existing carbonaceous materials, such as hydrogenated amorphous carbon (HACs), polycyclic aromatic hydrocarbons (PAHs), or PAH-like structures, could also be important formation routes (12, 19, 20). Indeed, such photochemical processing could work in tandem with CNG formation to produce

ASTRONOMY

Significance

We experimentally study the processes that result in fullerene formation in oxygen- and hydrogen-rich carbon gas. Metallofullerenes are found to form as readily as empty cages and thus, like fullerenes, should be important constituents of (circum)stellar/interstellar space. Element trapping by metallofullerene formation is shown to be selective and rapid, which can explain long-standing astrophysical puzzles such as the anomalous element enrichment of stardust. Infrared spectroscopic signatures are simulated to provide an observational test for metallofullerenes in space. Further, energetic reactions between larger polycyclic aromatic hydrocarbons (PAHs) and fullerenes are established form stable classes of complex molecules that hold high astrochemical importance. Bottom-up fullerene growth is also demonstrated to result from PAH processing, another potentially important extraterrestrial formation mechanism.

Author contributions: P.W.D., C.P.E., A.G.M., and H.W.K. designed research; P.W.D. and J.-J.A. performed research; N.K.K., J.P.Q., and G.T.B. contributed new reagents/analytic tools; P.W.D., J.-J.A., C.P.E., A.G.M., and H.W.K. analyzed data; and P.W.D., J.-J.A., C.P.E., A.G.M., and H.W.K. wrote the paper.

The authors declare no conflict of interest.

[1]To whom correspondence may be addressed. E-mail: pdunk@chem.fsu.edu, chris.ewels@cnrs-imn.fr, marshall@magnet.fsu.edu, or kroto@chem.fsu.edu.

This article contains supporting information online at www.pnas.org/lookup/suppl/doi:10.1073/pnas.1315928110/-/DCSupplemental.

C_{60} and other larger fullerenes in lower-energy conditions, outside of stellar environments. We note that because energetic barriers are low or nonexistent for incorporation of C and C_2 into closed cages and carbon catalyzed bond rearrangements (17), CNG formation should also be possible in circumstellar environments, such as planetary nebula.

Many investigations into the astronomical origin of these hollow caged molecules are currently under way. By contrast, little consideration has been given to endohedral metallofullerenes, which are cages that encapsulate metals and other elements, as relevant astrochemical species. Understanding how large carbon molecules can form in the hostile environments of stellar outflows is a central issue that should offer valuable information on the origin and cosmic role of fullerenes. Critical insight into that problem can be achieved by study of the key processes and resulting molecular products formed through carbon condensation reactions in high-energy oxygen- and hydrogen-rich environments.

Herein, we explore carbon condensation and interaction with Na under highly energetic conditions by use of a pulsed supersonic cluster source (21), analyzed by ultrahigh-resolution Fourier transform ion cyclotron resonance (FT-ICR) mass spectrometry (22) and supported by density functional theory (DFT) calculations. We show that the Na atom and ion appears to catalyze the nucleation of fullerenes in oxygen- and hydrogen-rich environments to produce $Na@C_{60}$, as well as other $Na@C_{2n}$ (in which C_{2n} is an even-numbered fullerene cage), in high relative abundance. Based on the experimental results, we propose that metallofullerene formation is the basic process that traps radioactive ^{22}Na in condensing carbon of stellar environments, such as supernova ejecta, before decay into highly inert ^{22}Ne. The same atom trapping and growth processes occur for many other elements, thus many different metallofullerene species may impact astrochemical processes. Accordingly, the application of metallofullerenes to celestial roles could unravel many long-standing astrophysical puzzles, as well as provide perspective on large carbon molecule formation in space. Finally, gas-phase interaction of fullerenes and PAHs are probed under energetic conditions to provide fundamental insight into fullerene astrochemistry and formation of carbonaceous dust.

Results and Discussion

Formation of $Na@C_{60}$ from Carbon Gas. The conditions of supernova ejecta guarantee that gaseous atoms and ions are the starting point to molecular growth and grain formation (2, 3). Condensation then occurs after the gas cools to the appropriate condensation temperature. Likewise, laser ablation of a carbon target rod by use of a pulsed supersonic cluster source generates carbon vapor consisting of gaseous atoms and ions (17). Condensation occurs only after carbon gas cools from thousands of degrees Celsius to the appropriate condensation temperature. The presence of helium cools the carbon gas to condensation temperature on a convenient experimental time scale. Thus, high-energy gas-phase carbon chemistry can be experimentally probed. The same carbon chemistry should operate in other highly energetic environments, such as stellar ejecta.

In order for metallofullerenes, such as $Na@C_{60}$, to be astrochemically viable, the endohedral atom must be an element that readily incorporates within cages. Fullerenes are known, however, to encapsulate only particular elements in condensing carbon vapor (23). Whereas some group I elements have successfully been encapsulated, there have been no experimental investigations of Na in condensing carbon. The only reports of $Na@C_{60}$ formation are through ion implantation into preexisting C_{60} films at extremely low yields (24). Experimental constraints have likely precluded the Na–carbon condensation system from previous study. For example, unambiguous identification of $Na@C_{60}$ and other $Na@C_{2n}$ requires detection of isotopic distributions, and thus the relevant ~6.5-mDa mass differences between empty cages and Na-containing metallofullerenes must be resolved. Analysis by the present 9.4 T FT-ICR mass spectrometer provides ultrahigh resolution and high mass accuracy, and overcomes that experimental challenge (22, 25).

To probe the ability of Na to nucleate metallofullerene formation in carbon plasma, a Na-doped carbon rod (1.0 atom % Na) was subjected to laser ablation (~35 $mJ \cdot cm^{-2}$ fluence or 5 mJ per pulse) under a 10-psi He flow. Because ^{22}Na is not available for experimental study, ^{23}Na is used. Both isotopes exhibit the same essential chemical reactivity and kinetics, and thus ^{23}Na can be used to accurately elucidate interaction of ^{22}Na with carbon plasma. Fig. 1 shows the cluster cations generated under conditions that yield empty-caged fullerenes. The empty-caged species are observed, as expected, but an entire family of carbon clusters containing a single Na atom is also present. $Na@C_{60}$ forms as the most abundant species, followed by $Na@C_{70}$. All $Na@C_{2n}$ are unequivocally resolved from the "overlapping" empty cages. For example, as shown in Fig. 1, $Na@C_{60}$ is clearly resolved from empty cage C_{62}, definitively showing that $Na@C_{60}$ spontaneously forms in condensing carbon. Fragmentation experiments unambiguously confirm that $Na@C_{60}$ and all other $Na@C_{2n}$ cluster ions formed are endohedral metallofullerenes (Fig. S1). The investigations also reveal that the $Na@C_{60}$ cluster is highly robust with respect to thermal dissociation.

The carbon cage isomer of $Na@C_{60}$ is almost certainly I_h-C_{60}. Note that the I_h-C_{60} cage has been structurally confirmed to encapsulate another group I element, $Li@I_h$-C_{60} (26). I_h-C_{60} is the fullerene most resistant to reaction with atomic and diatomic carbon (17). Consequently, C_{60} is a kinetic obstacle in CNG from smaller to larger fullerenes, resulting in its dominant production in condensing carbon. The observed distribution of $Na@C_{2n}$ (Fig. 1, *Inset*) provides strong agreement for that formation path with regard to Na-containing cages and thus the icosahedral cage structure for $Na@C_{60}$, which obeys the isolated pentagon rule (27). Quantum chemical calculations show that Na preferentially resides 1.03–1.06 Å from the center of the icosahedral cage (Fig. 1). Interaction between the encapsulated Na atom and the cage is weak, with 1.2 electrons (e) charge transfer from Na to the cage for neutral $Na@C_{60}$. The molecule should be ionized in the energetic and radioactive environment of supernovae, making our detection of a stable $Na@C_{60}$ cation highly relevant. Our DFT calculations indicate $Na@C_{60}^+$ exhibits nearly identical structure to $Na@C_{60}$.

Metallofullerene and Fullerene Formation in Oxygen- and Hydrogen-Rich Environments. Oxygen may be present when astrochemical carbon condensation reactions take place in stellar ejecta (2–4, 28, 29). For instance, mixing of element-rich concentric shells or zones likely occurs in supernova ejecta, and the carbon-rich zones may inherently possess oxygen. Further, oxygen can be present in other important stellar outflows that are thought to be major sources of carbon molecules and dust: for example, asymptotic giant branch (AGB) and carbon stars. Therefore, metallofullerene and fullerene formation in oxygen-rich environments was experimentally probed. Fig. S2 shows the cluster cations generated from Na-seeded carbon vapor under a 10-psi flow of combined oxygen and helium (5 psi O_2 and 5 psi He); all other parameters are unchanged. Endohedral metallofullerenes and fullerenes are still observed, with $Na@C_{60}$ forming as the dominant metallofullerene and C_{60} as the dominant empty cage. The overall ion abundance declined by an order of magnitude compared with formation in pure He, revealing that although oxygen reduces the efficiency of fullerene formation, its presence is not completely detrimental. Surprisingly, $Na@C_{60}$ and the $Na@C_{2n}$ metallofullerene family now exhibit an increased relative abundance to the empty cages (i.e., the abundance of the empty cages appears to have declined to a greater extent than that of the metallofullerenes). In the presence of oxygen, carbon gas available for clustering can be removed by formation of CO and other small molecules, leading to a decrease in fullerene production. Another possibility is that smaller carbon structures, mostly linear chains and rings (30, 31), can be oxidized, thereby lowering the production of the smallest fullerene(s) that grow

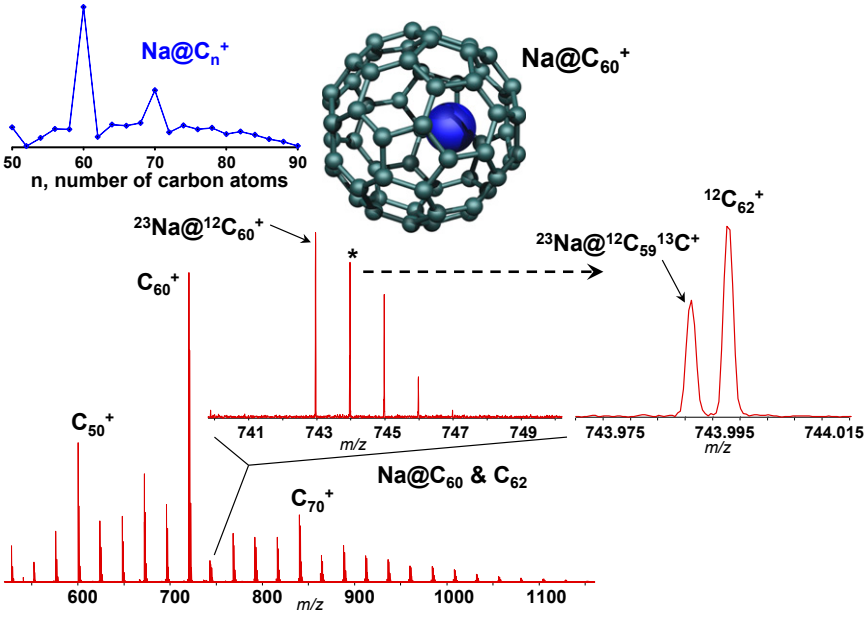

Fig. 1. FT-ICR mass spectrum of cluster cations that spontaneously form in condensing carbon vapor seeded with Na (10 psi He gas flow, ~35 mJ·cm^{-2} fluence). (*Insets*) Na@C_{60} clearly resolved from empty C_{62} and the relative abundance of Na@C_{2n} species.

into the larger fullerenes, such as Na@C_{60} and C_{60}. Similar condensation distributions are observed when hydrogen gas is substituted for oxygen, except that the changes in relative abundances are less significant (Fig. S2).

To more clearly elucidate the effects of oxygen, preexisting I_h-C_{60} was exposed to carbon vapor at a high pressure of pure oxygen gas, as shown in Fig. S3. It is clearly demonstrated that C_{60} readily grows into larger fullerenes by the CNG formation process. The observed low-abundance cages smaller than C_{60} in spectrum are fragmentation products of the original "starting material" C_{60}, due to direct interaction with the laser during vaporization. By contrast, when Fig. S3 is compared with growth of preexisting C_{60} in carbon gas without oxygen or even in the presence of pure hydrogen (17), less growth occurs. Similar behavior is expected for the Na-containing metallofullerene species. The lack of fullerene cage destruction by oxidation during growth in oxygen suggests the observed reduction in growth of C_{60} into larger fullerenes is most likely caused by free carbon becoming trapped as CO and other smaller reactive structures. The present instrument is not configured for detection of very low-mass species, such as CO. Previous reports, however, show that oxygen substantially affects small carbon clusters, with CO forming in high abundance from carbon vapor under the flow of oxygen (32). Nevertheless, the present results clearly demonstrate that carbon cages grow in oxygen-rich environments of carbon gas.

Because C_{60} is demonstrated to readily grow into larger fullerenes, oxygen must affect initial formation of the smallest fullerenes most significantly, rather than cage growth, during formation from carbon gas without preexisting fullerenes. Oxidation of small fullerene precursors and reduced availability of carbon would decrease small fullerene formation efficiency. However, the ability of metals to actively nucleate carbon (18) should provide a mechanistic advantage for formation of the smallest Na@C_{2n}, which then (even in the presence of oxygen) grow into larger Na@C_{2n}. That process can explain the significant change in relative abundance of Na@C_{2n} and C_{2n} in Fig. S2. The ability of carbon to cluster at a high temperature surely permits preferential reaction of cages with carbon gas rather than oxygen (30). In addition, the highly radioactive environment of supernovae could permit free carbon for clustering even under conditions where O > C, due to CO dissociation (33) to yield fullerenes via CNG formation.

Selective Capture of Na During Carbon Condensation. Another fascinating problem with regard to presolar carbonaceous grains is that ^{20}Ne should be more than five orders of magnitude more abundant than ^{22}Na in the Ne/O zone of supernovae where radiogenic ^{22}Na should be produced (4, 29). Despite that scenario, radiogenic ^{22}Na (i.e., ^{22}Ne) is significantly more abundant than ^{20}Ne in carbonaceous grains of supernovae origin. Indeed, nearly pure ^{22}Ne can be observed from grains. To confirm that the trapping process involves Na rather than any Ne isotope, the condensation of Na-seeded (1.0% Na) carbon gas in a ^{20}Ne-rich (10 psi, natural abundance Ne, >90% ^{20}Ne) environment was investigated. Na@C_{60} is observed to form high relative abundance in the presence of these elements and, importantly, no detectable ^{20}Ne (nor any other Ne isotope) is incorporated into any carbon cage (Fig. S4). Thus, Na trapping by carbon cages is proven to be selective, which is critical to achieve the enrichment of ^{22}Ne (via ^{22}Na) in supernovae-originating carbon stardust. We note that fullerenes have been claimed to be found in the Murchison meteorite, a carbonaceous chondrite, and that extraterrestrial He was possibly trapped in the some of the cages (34); however, that result is still awaiting confirmation.

Gas-Phase Reaction of Fullerenes with PAHs Under Energetic Conditions. Presolar graphitic grains exhibit distinct average morphologies. Transmission electron microscopy (TEM) studies suggest that the nanostructure consists of graphene-like carbon networks with no long-range order or turbostratic graphite, and also randomly oriented planar networks of hexagonal carbon rings, perhaps up to 3–4 nm in size. Both of these morphologies are essentially PAH skeletal and graphene-like structures (35). Higher degrees of graphitization can be found in the exterior regions of some high-density carbon grains; however, these grains are more likely to originate from AGB stars than supernovae. In order for ^{22}Na@C_{60}, ^{22}Na@C_{70}, and the many other Na-containing metallofullerenes to enrich carbon stardust, they must incorporate into larger carbon aggregates or growing grains and thus react with the observed graphene-like networks or PAH skeletal structures. To probe that formation process, C_{60} and C_{70} were exposed to coronene under energetic conditions in the gas phase by vaporization of a fullerene–PAH target. Coronene, a planar network of hexagonal rings, is an astrochemically important molecule (36) and serves as a basic test for reactivity of larger hexagonal networked graphene-like structures. Furthermore, stellar outflows are also thought to be a major source of PAHs found in the universe

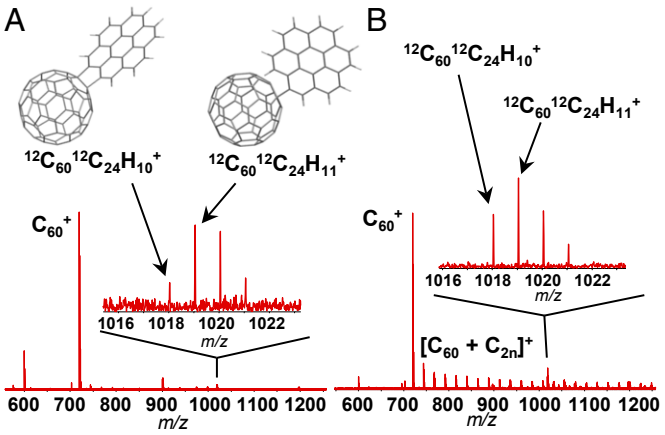

Fig. 2. Cluster cations formed by interaction of C_{60} and coronene in the gas phase under (*A*) energetic (20 mJ·cm^{-2}) and (*B*) higher-energy conditions (~35 mJ·cm^{-2}).

(37). Thus, reaction of PAHs with fullerenes provides additional insight into fundamental astrochemistry between these two important classes of large cosmic molecules. For example, a better understanding of the carbon structures that produce the enigmatic diffuse interstellar bands (DIBs) can also be achieved by such investigations (38). Very recently, it has been shown that small PAHs, such as anthracene, can form a Diels–Alder cycloaddition product in the gas phase (39). Although these particular fullerene–anthracene adducts may not be stable enough to exist in circumstellar or interstellar environments, more complex fullerene–PAH products (i.e., fullerene adducts with larger PAHs) are expected to be stable and thus could be present in space.

Because the two most abundant Na-containing metallofullerenes, Na@C_{60} and Na@C_{70}, possess the same structural arrangement of carbon atoms as I_h-C_{60} and D_{5h}-C_{70}, the reactivity of those empty cages can be used to directly infer the relative gas-phase reaction of PAHs with the Na-encapsulated equivalents. Further, those empty cages should also be present under conditions that form metallofullerenes in stellar ejecta. Gas-phase interaction of fullerenes and PAHs are achieved by laser vaporization of a target comprised of the two species. Fig. S5 shows the gas-phase reaction product anions of C_{60} or C_{70} with coronene ($C_{24}H_{12}$) under energetic conditions (20 mJ·cm^{-2} or 3 mJ per pulse, 10 psi He). For both fullerenes, a molecular species consisting of the respective fullerene and $C_{24}H_{11}{}^{-}$, singly H-abstracted coronene, are clearly formed. C_{70} is observed to be much more reactive than C_{60}. In addition, a second cluster anion species that is comprised of a fullerene with coronene that has lost two H atoms is observed at much lower abundance for C_{70}. Interestingly, there are also formation products that correspond to larger fullerene cages. Those fullerene species certainly form by carbon incorporation into C_{60} or C_{70} through the CNG formation mechanism. Fullerene-incorporated carbon must originate from the breakdown of the PAHs because almost no fullerene fragmentation is observed. These observations strongly indicate that processing of circumstellar or interstellar PAHs can result in growth of fullerenes by CNG formation, which may be an important cosmic fullerene production route. That observation also indicates that a high temperature was achieved and thus the combined fullerene–PAH molecules are quite stable in the gas phase.

The resulting positive ion clusters exhibit even more remarkable gas-phase product spectra. Fig. 2 shows the cluster cations produced from gas-phase interaction of C_{60} and coronene by vaporization (20 mJ·cm^{-2}) of a C_{60}–coronene target. $C_{60}C_{24}H_{11}{}^{+}$ is observed as a primary reaction product, but an appreciable abundance $C_{60}C_{24}H_{10}{}^{+}$ is also present. Under higher-energy conditions (~35 mJ·cm^{-2}), CNG formation of C_{60} into larger fullerenes occurs much more substantially, and the fullerene–PAH molecular products exhibit much higher abundance. Further, the reaction of doubly H-abstracted coronene with C_{60} occurs to a greater extent, as shown in Fig. 2, by the change in relative abundance for the dominant isotope species of $C_{60}C_{24}H_{10}{}^{+}$ and $C_{60}C_{24}H_{11}{}^{+}$. Under both conditions, clusters corresponding to multiples of coronene at *m/z* ~600, ~900, and ~1,200 are observed (*SI Materials and Methods*), with the clusters containing three or more units losing several H atoms from the parent $C_{24}H_{12}$ PAHs. Under these highly energetic conditions, the negative cluster ions feature a similar increase in CNG of C_{60} into larger fullerenes (Fig. S5).

Fig. 3 shows the positive ion mass spectrum for reaction of C_{70} and coronene (at 20 mJ·cm^{-2}). Notably, C_{70} is more reactive to H-abstracted coronenes, $C_{24}H_{10}$ and $C_{24}H_{11}$, than C_{60}. At higher energy (~35 mJ·cm^{-2}), a similar increase in CNG of C_{70} into larger fullerenes occurs as observed for C_{60}. Some of the C_{70} is hydrogenated after gas-phase interaction with $C_{24}H_{12}$. By contrast, no hydrogenated C_{60} is observed under similar conditions. Thus, hydrofullerenes may result from PAH processing. Further, the results also suggest the possibility that certain fullerenes may be important for H abstraction of PAHs. Interestingly, a significant abundance of even more complex clusters also form that correspond to reaction of C_{70} with two H-abstracted coronene-based molecular units (Fig. S6).

To elucidate the structure of these newly formed species, fragmentation studies of the fullerene–PAH product cations were performed. The highly abundant C_{70}–PAH reaction products ($C_{70}C_{24}H_{10}{}^{+}$ and $C_{70}C_{24}H_{11}{}^{+}$) were isolated and then fragmented by collision-induced dissociation by means of sustained off-resonance irradiation (22), as shown in Fig. S7. Upon high thermal excitation, intact C_{70} results with no other fullerene cage fragmentation products. Importantly, intact $C_{24}H_{11}{}^{+}$ and $C_{24}H_{10}{}^{+}$ are unambiguously observed as the only other fragmentation products, supporting the proposed structures depicted in Figs. 2 and 3. After thermal excitation and fragmentation of the parent ions, $C_{70}C_{24}H_{10}{}^{+}$ is the only surviving parent ion. Thus, the $C_{70}C_{24}H_{10}{}^{+}$ molecule is much more stable than $C_{70}C_{24}H_{11}{}^{+}$. That observation provides strong support for two sites of covalent bonding between C_{70} and $C_{24}H_{10}$ in the corresponding parent structure, whereas the singly

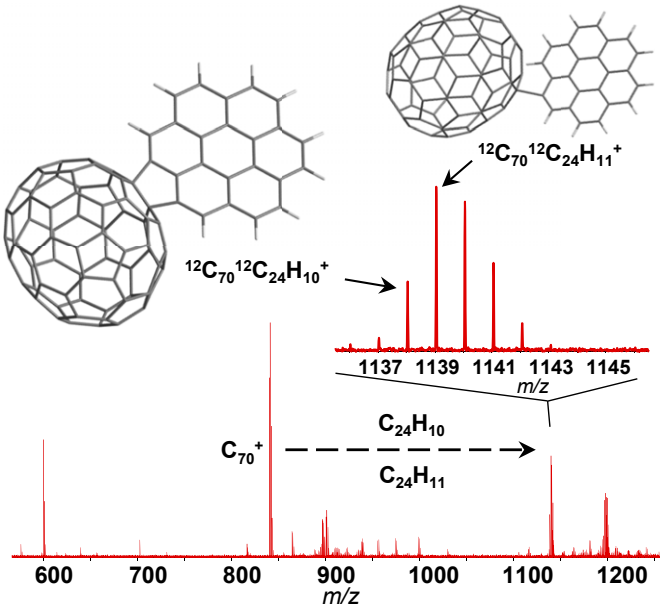

Fig. 3. Cluster cations formed by interaction of C_{70} and coronene in the gas phase under energetic conditions (20 mJ·cm^{-2}).

H-abstracted $C_{24}H_{11}$ molecule can, at most, exhibit a single covalent bond to a fullerene. The same fragmentation PAH clusters ($C_{24}H_{11}$+ and $C_{24}H_{10}^{+}$) are observed for C_{60}–PAH molecules ($C_{60}C_{24}H_{10}^{+}$ and $C_{60}C_{24}H_{11}^{+}$), and thus exhibit similar bonding features as the C_{70}–PAH cluster ions. Further experimental support for covalent bonding is given by $C_{59}NC_{24}H_{11}$, which features a single covalent bond between a carbon atom of the fullerene cage and singly H-abstracted coronene (40). We find that interaction of C_{60} or C_{70} with smaller PAHs (anthracene, naphthalene) do not exhibit remarkable reaction product spectra, because only extremely low-abundance fullerene–PAH products are observed. Small PAHs may be much less stable than coronene under the present energetic conditions (41, 42).

If the graphene-like or PAH skeletal networks observed in presolar grains form directly in supernova ejecta (33), the present work shows that those structures should react with fullerenes and metallofullerenes present. A metallofullerene or fullerene should even be able to react with a preexisting large carbon grain to permit incorporation as well.

Several plausible routes to the formation of carbon stardust that incorporate ^{22}Na through element capture by metallofullerene formation are possible based on these experimental observations. ^{22}Na can decay to ^{22}Ne before or after inclusion into a carbon aggregate, because some fullerenes appear to be rather stable toward gamma-ray irradiation (43), and Ne@C_{60} has been previously demonstrated to be stable (44). Further, metamorphosis is likely to occur to any carbon grain that is injected into the ISM. Thus, newly formed carbon aggregates or grains in stellar ejecta could initially be comprised of large molecules or nanostructures consisting of fullerenes and polycyclic carbon sheets, and thereafter, phase transformations could alter the carbon nanostructure (45, 46). In fact, metallofullerenes have been shown to graphitize and exhibit other phase transitions upon heating (47). The metamorphosis of C_{60} and other fullerenes is known and exhibit astrochemically relevant structural transitions (48). It is interesting to note that the density of metamorphized C_{60} falls into the density range of supernovae-originating carbon grains (48).

Effect of Metal Encapsulation on IR Spectra of C_{60}. The results show that Na@C_{2n} and C_{2n} should react with polycyclic carbon, graphene-like networks and PAHs, and therefore can be incorporated into a carbon grain or participate in astrochemistry in circumstellar or interstellar space. The C_{60} cage, however, is shown to be much less reactive than other fullerenes. Consequently, it may be possible for M@C_{60} (M indicates metal) metallofullerenes, such as Na@C_{60} or empty-cage C_{60}, to survive stellar ejecta and escape into interstellar space. Thus, molecular M@C_{60} in circumstellar and interstellar space may be spectroscopically observable in the gas phase or on the surface of a grain. To determine the change in IR absorption that results from metal encapsulation, further quantum chemical investigations of Na@C_{60} were performed.

Metallofullerenes are described by an ionic model, in which electrons from the encapsulated metal transfer to the carbon cage (18). Because our Mulliken charge analysis shows a transfer of 1.2 electrons from Na to the C_{60} cage, the neutral Na@C_{60} is better described as the indissociable ion pair, $Na^{+}@C_{60}^{-}$, in agreement with previous investigations (49, 50). To separate effects due explicitly to Na and thus determine how charge transfer changes C_{60} absorption, vibrational modes for C_{60}, Na@C_{60}, and C_{60}^{-} were calculated. Most of the spectral features of Na@C_{60} are reproduced in the C_{60}^{-} spectrum, as shown in Fig. 4. The IR-active vibrational modes for C_{60} and Na@C_{60} are given in Table S1. The negatively charged fullerenes have much higher absorption intensities (a factor of ~10) compared with the corresponding neutral. The lower IR mode frequencies, T_{1u}– (1–3), are insensitive to charge state, whereas the T_{1u}– (4) mode exhibits a significant shift (Fig. S8). Furthermore, with increasing charge state, those lower modes remain relatively unaffected, whereas the T_{1u}– (4) continues to shift appreciably (Fig. S8). Introducing electronic charge to the lowest unoccupied molecular orbital (LUMO) of C_{60} breaks system symmetry and activates previously IR-silent modes, notably a distinctive higher peak (1,543 cm^{-1}) derived from the Hu (7) and Hg (8) modes at 1,557 and 1,554 cm^{-1} (*SI Materials and Methods*, Table S1, and Fig. S9), consisting of oscillations in opposing pentagons of the cage. The shift of that new mode with increasing negative charge follows a similar trend to the T_{1u}– (4) mode. Though the calculated spectrum is for a single Na@C_{60} configuration, Na motion within the cage is likely to broaden the observed peaks. Given that the primary effect of endofullerene metal addition on IR absorption is simply charge transfer to the fullerene cage, the calculated peak shifts enable estimation of charge transfer in other endofullerene species or, alternatively, to estimate approximate IR peak positions based on the endohedral metal oxidation state.

Conclusions

The explicit demonstration that Na can nucleate carbon to form metallofullerenes, such as Na@C_{60}, under highly energetic conditions in oxygen- and hydrogen-rich environments strongly indicates that related endohedral carbon species will form in some stellar outflows, such as supernova ejecta. Thus, the long-standing mystery of how ^{22}Na, observed as the anomalous ^{22}Ne in carbon grains, enriches carbon dust can be explained physically by metallofullerene trapping. Dust is known to form ~350–600 d after a supernova explosion, and the half-life of ^{22}Na is short; therefore, the present demonstration of spontaneous and rapid metallofullerene element trapping is critical. Further, even after decay to highly inert ^{22}Ne, that element will remain trapped within carbon. The processes demonstrated for Na in this study occur for many other elements; consequently, many metallofullerenes species could potentially enrich stardust and could be used to understand other celestial processes. This study also serves as a benchmark for empty cage formation in stellar environments. Metallofullerene and fullerene formation, as indicated by this work, appear to agree with other factors that govern carbon dust condensation in supernova ejecta (28, 33). Furthermore, fullerenes also readily incorporate heteroatoms and other elements into their caged networks (51)–yet another possible fullerene-related route for the enrichment of stardust. The effect of metal encapsulation on IR absorption was investigated theoretically, which should help detect cosmic metallofullerenes. Interestingly, unidentified frequencies in IR spectra of fullerene-rich planetary nebula (11, 52) show notable coincidences to metallofullerenes due to the vibrational mode that becomes IR-active when a metal, such as Na, is encapsulated within C_{60}. This work also opens up the possibility that negatively charged cages may be present in certain fullerene-rich environments because the simulations show that they exhibit similar spectral features to neutral metallofullerenes.

To understand how fullerenes may aggregate or incorporate into carbon grains, the interaction of C_{60} and C_{70} with PAHs

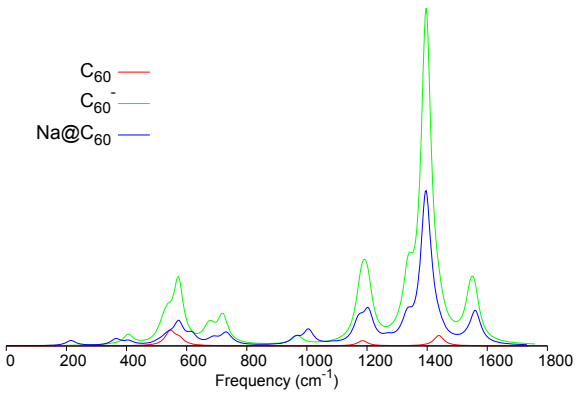

Fig. 4. Calculated IR spectra for Na@C_{60}, C_{60}^{-}, and C_{60}.

was investigated. Gas-phase reactions between H-abstracted coronene and C_{60} or C_{70} readily occur, and these species can be quite stable. Thus, fundamental reactions between PAHs and fullerenes are shown to produce a likely significant class of cosmic molecules that hold promise to explain other long-standing astronomical problems, such as identification of the carriers of DIBs and spectral emission features of other circumstellar and interstellar environments, and also provide insight into how fullerenes and metallofullerenes can enrich or integrate into carbon grains. Moreover, the CNG formation of fullerenes by the breakdown of PAHs is experimentally revealed in this work, which is likely an important process for circumstellar and interstellar fullerene production.

Materials and Methods

Cluster Source and 9.4 T Fourier Transform Ion Cyclotron Mass Spectrometry. All experiments were performed by laser vaporization (Nd:YAG laser, 532 nm) of Na carbon, C_{60}-coated carbon, or fullerene–PAH target rods by use of a pulsed supersonic cluster source and analyzed by a custom-built ultrahigh-resolution 9.4 T FT-ICR mass spectrometer (17, 18, 51). Detailed experimental descriptions are available in *SI Materials and Methods*.

Preparation of Na-Containing Carbon Target. The 12.7-mm diameter Na-doped rods were prepared by mixing graphite powder (99.999%) and $NaCO_3$ or NaCl to give a 1.0 atomic percent Na target material, which was subsequently molded into a target rod.

Preparation of Graphite–PAH Targets. A total of 500 μg of C_{60} (99.9%) or C_{70} (>99%) was dissolved in a minimal amount of toluene and applied to the surface of a 6.3-mm ground quartz rod. Next, 500 μg of PAH (coronene, anthracene, or naphthalene), dissolved in a minimal amount of toluene, was applied to the fullerene-coated quartz rod. The rod was then placed in the cluster source at base pressure (1×10^{-7} torr) for several hours before use to ensure removal of any residual solvent.

Growth of C_{60} in Oxygen Gas. A total of 500 μg of C_{60} (99.9%) was uniformly applied to the surface of a graphite rod (99.999%). Laser ablation was then performed under a flow of pure oxygen gas (99.999%).

Quantum Chemical Calculations. DFT calculations were performed by use of the Gaussian 09 code with B3LYP exchange correlation and a 6-311G basis set. Further details are given in *SI Materials and Methods*.

ACKNOWLEDGMENTS. This work was funded by National Science Foundation (NSF) Division of Materials Research (DMR) and Division of Chemistry (CHE) Grants NSF DMR-1157490 and CHE-1019193; the Florida State University Research Foundation; and Agence Nationale de la Recherche (ANR) Grant ANR-2010-BLAN-0819-04.

1. Amari S, Anders E, Virag A, Zinner E (1990) Interstellar graphite in meteorites. *Nature* 345(6272):238–240.
2. Clayton DD, Nittler LR (2004) Astrophysics with presolar stardust. *Annu Rev Astron Astrophys* 42:39–78.
3. Zinner E (1998) Stellar nucleosynthesis and the isotopic composition of presolar grains from primitive meteorites. *Annu Rev Earth Planet Sci* 26:147–188.
4. Amari S (2009) Sodium-22 from supernovae: A meteorite connection. *Astrophys J* 690(2):1424–1431.
5. Clayton DD (1975) Na-22, Ne-E, extinct radioactive anomalies and unsupported Ar-40. *Nature* 257(5521):36–37.
6. Matsuura M, et al. (2011) Herschel detects a massive dust reservoir in supernova 1987A. *Science* 333(6047):1258–1261.
7. Sugerman BEK, et al. (2006) Massive-star supernovae as major dust factories. *Science* 313(5784):196–200.
8. Dunne L, Eales S, Ivison R, Morgan H, Edmunds M (2003) Type II supernovae as a significant source of interstellar dust. *Nature* 424(6946):285–287.
9. Kroto HW, Heath JR, Obrien SC, Curl RF, Smalley RE (1985) C_{60}- Buckminsterfullerene. *Nature* 318(6042):162–163.
10. Kroto HW, Jura M (1992) Circumstellar and interstellar fullerenes and their analogs. *Astron Astrophys* 263(1-2):275–280.
11. Cami J, Bernard-Salas J, Peeters E, Malek SE (2010) Detection of C_{60} and C_{70} in a young planetary nebula. *Science* 329(5996):1180–1182.
12. García-Hernández DA, et al. (2010) Formation of fullerenes in H-containing planetary nebulae. *Astrophys J* 724(1):L39–L43.
13. García-Hernández DA, Rao NK, Lambert DL (2011) Are C_{60} molecules detectable in circumstellar shells of R Coronae Borealis stars? *Astrophys J* 729(2):126.
14. Gielen C, Cami J, Bouwman J, Peeters E, Min M (2011) Carbonaceous molecules in the oxygen-rich circumstellar environment of binary post-AGB stars C_{60} fullerenes and polycyclic aromatic hydrocarbons. *Astron Astrophys* 536, A54.
15. Sellgren K, et al. (2010) C_{60} in reflection nebulae. *Astrophys J* 722(1):L54–L57.
16. Zhang Y, Kwok S (2011) Detection of C_{60} in the protoplanetary nebula Iras 01005+7910. *Astrophys J* 730(2):126.
17. Dunk PW, et al. (2012) Closed network growth of fullerenes. *Nat Commun* 3:855.
18. Dunk PW, et al. (2012) The smallest stable fullerene, M@C_{28} (m = Ti, Zr, U): Stabilization and growth from carbon vapor. *J Am Chem Soc* 134(22):9380–9389.
19. Micelotta ER, et al. (2012) The formation of cosmic fullerenes from arophatic clusters. *Astrophys J* 761(1):35.
20. Berné O, Tielens AGGM (2012) Formation of Buckminsterfullerene (C60) in interstellar space. *Proc Natl Acad Sci USA* 109(2):401–406.
21. Duncan MA (2012) Invited review article: Laser vaporization cluster sources. *Rev Sci Instrum* 83(4):041101.
22. Marshall AG, Hendrickson CL, Jackson GS (1998) Fourier transform ion cyclotron resonance mass spectrometry: A primer. *Mass Spectrom Rev* 17(1):1–35.
23. Lu X, Feng L, Akasaka T, Nagase S (2012) Current status and future developments of endohedral metallofullerenes. *Chem Soc Rev* 41(23):7723–7760.
24. Tellgmann R, Krawez N, Lin SH, Hertel IV, Campbell EEB (1996) Endohedral fullerene production. *Nature* 382(6590):407–408.
25. Cooper HJ, Hendrickson CL, Marshall AG, Cross RJ, Jr., Saunders M (2002) Direct detection and quantitation of He@C_{60} by ultrahigh-resolution Fourier transform ion cyclotron resonance mass spectrometry. *J Am Soc Mass Spectrom* 13(11):1349–1355.
26. Aoyagi S, et al. (2010) A layered ionic crystal of polar Li@C($_{60}$) superatoms. *Nat Chem* 2(8):678–683.
27. Kroto HW (1987) The stability of the fullerenes C_{24}, C_{28}, C_{32}, C_{36}, C_{50}, C_{60} and C_{70}. *Nature* 329(6139):529–531.
28. Travaglio C, et al. (1999) Low-density graphite grains and mixing in type II supernovae. *Astrophys J* 510(1):325–354.
29. Woosley SE, Heger A, Weaver TA (2002) The evolution and explosion of massive stars. *Rev Mod Phys* 74(4):1015–1071.
30. Van Orden A, Saykally RJ (1998) Small carbon clusters: Spectroscopy, structure, and energetics. *Chem Rev* 98(6):2313–2357.
31. von Helden G, Gotts NG, Bowers MT (1993) Experimental evidence for the formation of fullerenes by collisional heating of carbon rings in the gas-phase. *Nature* 363(6424):60–63.
32. Park SM, Moon JY (1998) Laser ablation of graphite in an oxygen jet. *J Chem Phys* 109(18):8124–8129.
33. Clayton DD, Liu WH, Dalgarno A (1999) Condensation of carbon in radioactive supernova gas. *Science* 283(5406):1290–1292.
34. Becker L, Poreda RJ, Bunch TE (2000) Fullerenes: An extraterrestrial carbon carrier phase for noble gases. *Proc Natl Acad Sci USA* 97(7):2979–2983.
35. Bernatowicz TJ, et al. (1996) Constraints on stellar grain formation from presolar graphite in the murchison meteorite. *Astrophys J* 472(2):760.
36. García-Hernández DA, et al. (2011) The formation of fullerenes: Clues from New C_{60}, C_{70}, and (possible) planar C_{24} detections in magellanic cloud planetary nebulae. *Astrophys J* 737(2):L30.
37. Cherchneff I, Barker JR, Tielens A (1992) Polycyclic aromatic hydrocarbon formation in carbon-rich stellar envelopes. *Astrophys J* 401(1):269–287.
38. García-Hernández DA, Diaz-Luis JJ (2013) Diffuse interstellar bands in fullerene planetary nebulae: The fullerene-diffuse interstellar bands connection. *Astron Astrophys* 550:L6.
39. García-Hernández DA, Cataldo F, Manchado A (2013) Infrared spectroscopy of fullerene C_{60}/anthracene adducts. *Mon Not R Astron Soc* 434(1):415–422.
40. Hauke F, et al. (2004) Molecular satellite dishes: Attaching parabolic and planar arenes to heterofullerenes. *Chem Commun (Camb)* (7):766–767.
41. Jennings E, Montgomery W, Lerch P (2010) Stability of coronene at high temperature and pressure. *J Phys Chem B* 114(48):15753–15758.
42. Le Page V, Snow TP, Bierbaum VM (2003) Hydrogenation and charge states of polycyclic aromatic hydrocarbons in diffuse clouds. II. Results. *Astrophys J* 584(1):316–330.
43. Cataldo F, Strazzulla G, Iglesias-Groth S (2009) Stability of C_{60} and C_{70} fullerenes toward corpuscular and gamma radiation. *Mon Not R Astron Soc* 394(2):615–623.
44. Saunders M, Jiménez-Vázquez HA, Cross RJ, Poreda RJ (1993) Stable compounds of helium and neon: He@C_{60} and Ne@C_{60}. *Science* 259(5100):1428–1430.
45. Tappe A, Rho J, Reach WT (2006) Shock processing of interstellar dust and polycyclic aromatic hydrocarbons in the supernova remnant N132D. *Astrophys J* 653(1):267–279.
46. Tappe A, Rho J, Boersma C, Micelotta ER (2012) Polycyclic aromatic hydrocarbon processing in the blast wave of the supernova remnant N132d. *Astrophys J* 754(2):132.
47. Zhao SX, et al. (2011) Structural change of metallofullerene: An easier thermal decomposition. *Nanoscale* 3(10):4130–4134.
48. Sundqvist B (1999) Fullerenes under high pressures. *Adv Phys* 48(1):1–134.
49. Schettino V, Pagliai M, Ciabini L, Cardini G (2001) The vibrational spectrum of fullerene C_{60}. *J Phys Chem A* 105(50):11192–11196.
50. Cardona M, Guntherodt G (2000) *Light Scattering in Solids VIII: Fullerenes, Semiconductor Surfaces, Coherent Phonons*, Topics in Applied Physics (Springer, Berlin), Vol 76, pp 1–26.
51. Dunk PW, et al. (2013) Formation of heterofullerenes by direct exposure of C_{60} to boron vapor. *Angew Chem Int Ed Engl* 52(1):315–319.
52. Bernard-Salas J, et al. (2012) On the excitation and formation of circumstellar fullerenes. *Astrophys J* 757(1):41.

Supporting Information

Dunk et al. 10.1073/pnas.1315928110

SI Materials and Methods

Cluster Source. The 6.3-mm diameter PAH–fullerene and Na–graphite 12.7-mm diameter target rods, which are simultaneously rotated and translated, were placed in cluster source blocks (1). A channel 2 mm in diameter and ∼8.5 mm in length runs from a pulsed valve (10–70 psi backing pressure, 800 μs pulse width) into the region containing the rod to introduce helium. A second channel 2 mm in diameter was directed into the target area to admit the laser beam. A channel 4 mm in diameter and ∼8.5 mm in length was located downstream from the target, aligned with the helium introduction channel to achieve confinement and clustering of the vapor produced. The gas then enters high vacuum and undergoes a free jet expansion. Vaporization of the target rod is achieved by a single laser pulse fired from a Nd:YAG laser (532 nm, 3–5 ns, 3 or 5 mJ per pulse, ∼1.5 mm beam diameter) in conjunction with the opening of a pulsed valve to admit He, Ne, and/or O_2. Mixtures were produced by filling the pulsed valve backing cylinder with the respective partial pressure of O_2, Ne, and He.

Ultrahigh Resolution 9.4 T Fourier Transform Ion Cyclotron Resonance Mass Spectrometry. All experiments were analyzed with a custom-built Fourier transform ion cyclotron resonance (FT-ICR) mass spectrometer based on a 9.4 T, 155-mm bore diameter actively shielded superconducting magnet, and conducted with positive and negative ions. The cluster source was housed in a source chamber (1×10^{-7} torr) evacuated by a large diffusion pump (3,000 L/s). Ions produced in the cluster source were transported to the ICR cell via three stages of differential pumping, each supplied with a turbomolecular pump to achieve ultrahigh vacuum (10^{-10} torr) in the ICR cell. After exiting the clustering region, the ions were skimmed into an octopole ion guide (175 $V_{p\text{-}p}$, 1.8 MHz, 570 mm length) and immediately transferred to a second octopole for ion accumulation. Ions were confined radially in the accumulation octopole (240 $V_{p\text{-}p}$, 2.8 MHz, 160 mm) by a time-varying electric field generated by a radiofrequency applied with 180° phase difference to adjacent rods and axially by the application of positive voltages to the end caps at the conductance limits at either side of the accumulation octopole. Helium gas was introduced through a pulsed valve to the accumulation octopole ($\sim 10^{-4}$ torr) to facilitate further ion cooling. After the accumulation of ions produced by 10 individual laser and helium pulse events, the ions were transferred by a third octopole (155 $V_{p\text{-}p}$, 2.2 MHz, 1,450 mm) to an open cylindrical ion trap (70 mm diameter, 212 mm long, aspect ratio ∼2) (2). The ions were accelerated to a detectable cyclotron radius by a broadband frequency sweep excitation (260 $V_{p\text{-}p}$, 150 Hz/μs, 3.6 down to 0.071 MHz) and subsequently detected as the differential current induced between two opposed electrodes of the ICR cell. Each acquisition was Hanning-apodized and zero-filled once before fast Fourier transform and magnitude calculation (3). Ten time-domain acquisitions were averaged. The experimental event sequence was controlled by a modular ICR data acquisition system (4).

Sustained Off-Resonance Irradiation–Collision-Induced Dissociation. Metallofullerenes, C_{60}–PAH product ions ($C_{60}C_{24}H_{11}^+$ and $C_{60}C_{24}H_{10}^+$), C_{70}–PAH product ions ($C_{70}C_{24}H_{11}^+$ and $C_{70}C_{24}H_{10}^+$), and all other ions of interest were isolated by applying a stored waveform inverse Fourier transform (SWIFT) event (5). The selected ions were then subjected to a 10-ms pulse of helium or argon directly injected into the ICR cell via a pulsed valve located outside the magnet bore, followed by 250-μs single-frequency excitation at 1 kHz off-resonance (5). After a 15- to 20-s delay to allow the system to reestablish base pressure, a broadband frequency sweep was carried out before detection. The mass spectrum was obtained from a single time-domain acquisition.

Quantum Chemical Calculations. Calculations were performed with density functional theory (DFT) by use of the Gaussian 09 code (6) with B3LYP exchange correlation and a 6-311G basis set. In each case, the structures are fully relaxed, and normal frequencies then calculated. Previous studies have shown that the Gaussian code gives generally good agreement with experimental vibrational frequencies with slight overestimation of values (7–9) from the 6-31G* basis set with the B3LYP hybrid exchange correlation functional (8). The overestimation was corrected with a scaling factor of 0.98 (10), correcting for basis set size and vibrational anharmonicity.

We compared here the 6-31G* and the large 6-311G basis set. The four IR active modes are well defined with both basis sets. However, the larger basis set provides a closer match to experiment values and was therefore adopted in the paper and Fig. 4 with a 0.99 scaling factor (Table S1). Given the good experimental agreement with 6-311G, we chose to use that basis set throughout and not apply any scaling factor.

For C_{60}, no differences were found between the "normal" and "very-tight" optimization criteria; hence we used normal optimization for $Na@C_{60}$. Different trial positions for the Na inside the cage were performed to find the lowest energy state. Mulliken analysis was used to determine charge transfer between the sodium atom and the cage.

1. Dunk PW, et al. (2012) Closed network growth of fullerenes. *Nat Commun*, 10.1038/ncomms1853.
2. Beu SC, Laude DA (1992) Open trapped ion cell geometries for Fourier-transform ion-cyclotron resonance mass-spectrometry. *Int J Mass Spectrom Ion Process* 112(2-3):215–230.
3. Marshall AG, Verdun FR (1990) *Fourier Transforms in NMR, Optical, and Mass Spectrometry: A User's Handbook* (Elsevier, Amsterdam).
4. Blakney GT, Hendrickson CL, Marshall AG (2011) Predator data station: A fast data acquisition system for advanced FT-ICR MS experiments. *Int J Mass Spectrom Ion Process* 306(2-3):246–252.
5. Marshall AG, Hendrickson CL, Jackson GS (1998) Fourier transform ion cyclotron resonance mass spectrometry: A primer. *Mass Spectrom Rev* 17(1):1–35.
6. Frisch MJ, et al. (2009) Gaussian 09, Revision A.1 (Gaussian, Inc., Wallingford, CT).
7. Bohnen KP, Heid R, Ho KM, Chan CT (1995) Ab-initio investigation of the vibrational and geometrical properties of solid C-60 and K3c60. *Phys Rev B* 51(9):5805–5813.
8. Schettino V, Pagliai M, Ciabini L, Cardini G (2001) The vibrational spectrum of fullerene C-60. *J Phys Chem A* 105(50):11192–11196.
9. Parker SF, et al. (2011) Complete assignment of the vibrational modes of C60 by inelastic neutron scattering spectroscopy and periodic-DFT. *Phys Chem Chem Phys* 13(17):7789–7804.
10. Rauhut G, Pulay P (1995) Transferable scaling factors for density-functional derived vibrational force-fields. *J Phys Chem* 99(10):3093–3100.

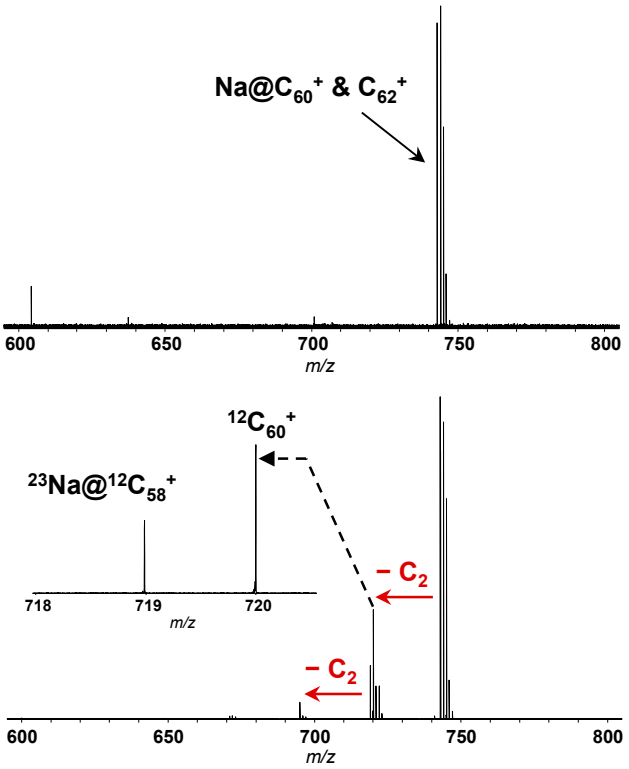

Fig. S1. Fragmentation of Na@C_{60}. SWIFT-isolated Na@C_{60} and C_{62} (*Upper*). Fragmentation pattern (*Lower*). Na@C_{60} is isolated along with C_{62} because their mass difference is too small to isolate individually. Na@C_{60} clearly fragments by C_2 loss with retention of Na after high thermal excitation. Only endohedral metallofullerenes exhibit C_2 loss with retention of a metal, whereas exohedrally bound metals dissociate at low thermal excitation without retention of the metal. All other Na@C_{2n} exhibit similar patterns. Thus, Na@C_{60} and all Na@C_{2n} are carbon cages that encapsulate a Na atom.

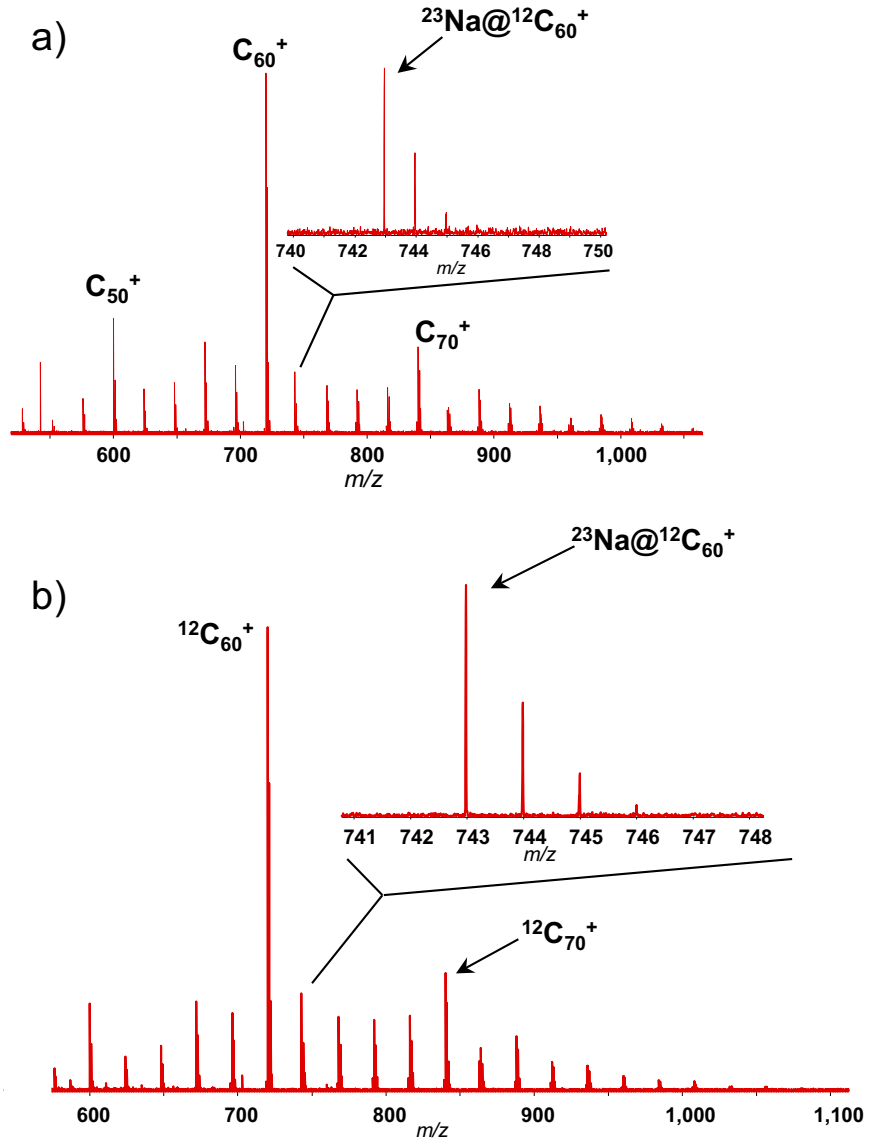

Fig. S2. (*A*) Condensation cluster cations resulting from condensation of carbon gas (without preexisting fullerenes) under oxygen-rich conditions (10-psi gas flow comprised of a partial pressure of 5 psi O_2 and 5 psi He combined, ~35 mJ·cm^{-2}). (*B*) Na@C_{60} and Na@C_{2n} formation from carbon vapor (without pre-existing fullerenes) under hydrogen-rich conditions (10-psi flow; 5 psi H_2 and 5psi He present simultaneously).

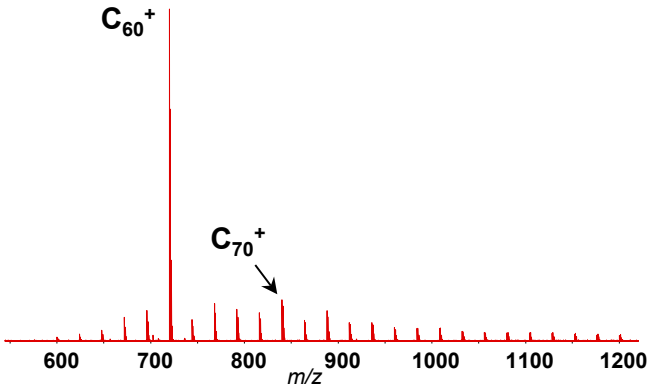

Fig. S3. Clusters resulting from growth of preexisting I_h-C_{60} exposed to carbon vapor at a high pressure of pure oxygen gas (50 psi O_2, ~35 mJ·cm^{-2}).

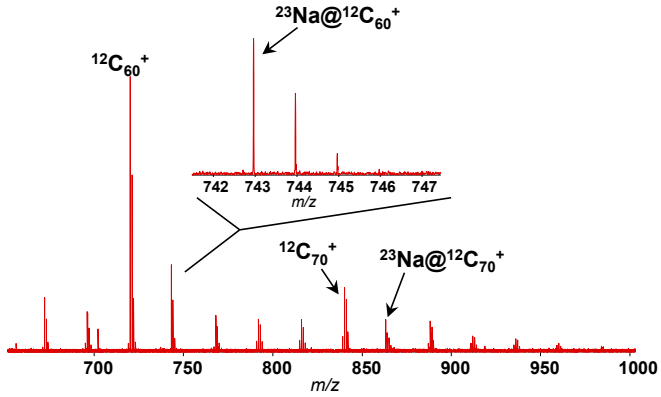

Fig. S4. Na@C_{60} and Na@C_{2n} formation from carbon vapor (without preexisting fullerenes) in pure Ne gas. Metallofullerene element trapping is demonstrated to be selective for Na because no isotopes of Ne are observed in any carbon cage. Interestingly, Na@C_{60} forms in higher relative abundance (as well as Na@C_{70}) under these conditions.

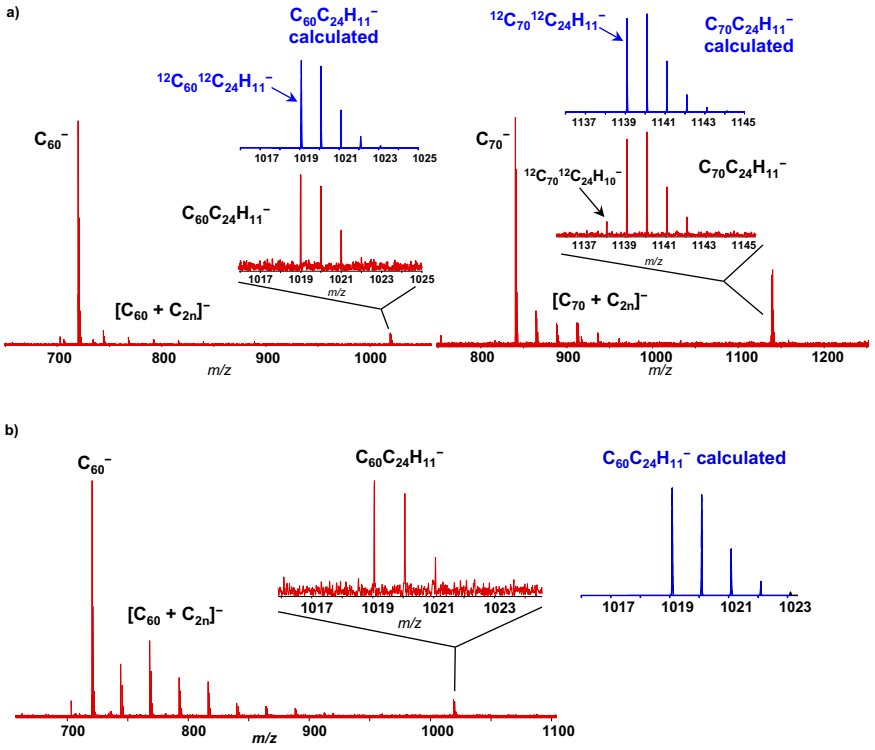

Fig. S5. (*A*) Cluster anions resulting from gas-phase interaction of (*Upper Left*) C_{60} and (*Upper Right*) C_{70} with coronene under energetic conditions (20 mJ·cm^{-2}). (*B*) Cluster anions resulting from gas-phase interaction of C_{60} and coronene under higher-energy (~35 mJ·cm^{-1}) conditions. The growth of C_{60} into larger fullerenes by closed network growth formation occurs to a greater extent, and the fullerene–PAH reactions product, $C_{60}C_{24}H_{11}^+$, exhibits higher abundance. However, the positive ion mass spectrum reveals that even more important reactions actually occur (Fig. S6).

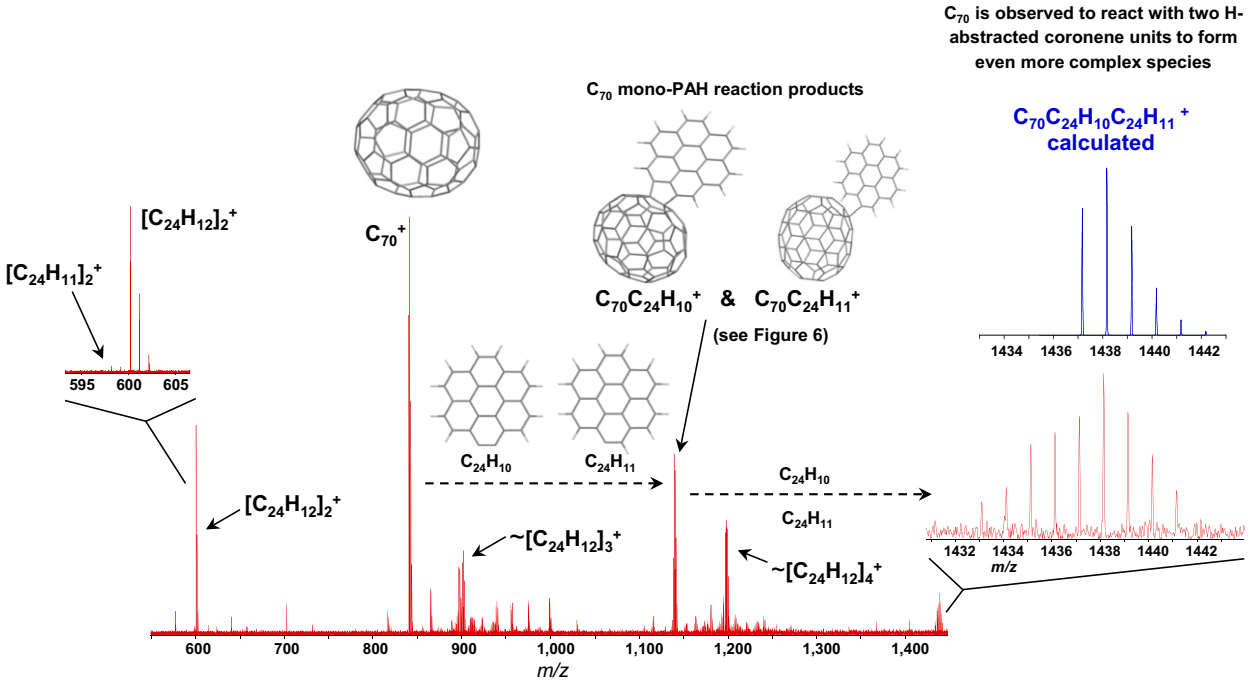

Fig. S6. Cluster cations formed by gas-phase interaction of C_{70} and coronene under energetic conditions (20 mJ·cm^{-1}). In addition to the formation of $C_{70}C_{24}H_{10}^+$ and $C_{70}C_{24}H_{11}^+$, additions of two coronene-based units to C_{70} are observed (*m/z* 1,433–1,411). The $C_{70}C_{24}H_{10}C_{24}H_{11}^+$ species appears to dominate, with other clusters exhibiting more H abstractions. $C_{70}(C_{24}H_{10})_2^+$ is also present. Fragmentation can be performed only with the positive ion species (see Fig. S7).

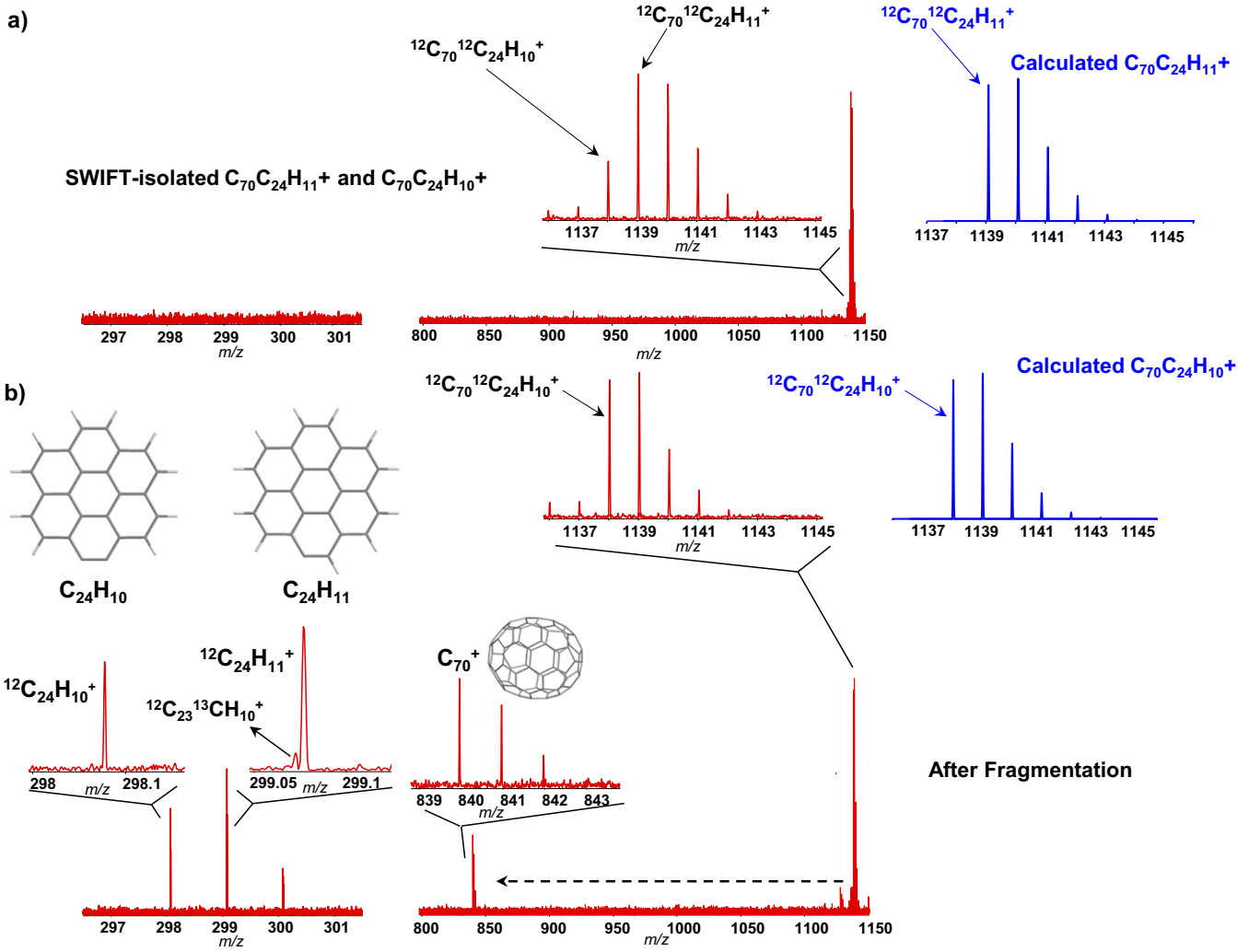

Fig. S7. Fragmentation spectrum of the $C_{70}C_{24}H_{11}$ and $C_{70}C_{24}H_{10}$ cations formed by interaction of C_{70} and coronene in the gas phase under energetic conditions. (*A*) SWIFT-isolated $C_{70}C_{24}H^{+}_{11}$ and $C_{70}C_{24}H^{+}_{10}$. (*B*) Dissociation of the isolated ions after thermal excitation by sustained off-resonance irradiation–collision-induced dissociation (SORI–CID). The only observed fragmentation products after dissociation by SORI–CID are C^{+}_{70}, $C_{70}C_{24}H^{+}_{10}$ and $C_{24}H^{+}_{11}$, clearly elucidating the components of the parent molecular ions. Before thermal dissociation, $C_{70}C_{24}H^{+}_{11}$ exhibits higher abundance than $C_{70}C_{24}H^{+}_{10}$; however, after high thermal excitation of the isolated fullerene–PAH molecules, $C_{70}C_{24}H^{+}_{10}$ is the only surviving species (with clusters corresponding to $C_{70}C_{24}H^{+}_{10-X}$, $X \leq 4$). That observation strongly supports the explanation that the $C_{70}C_{24}H^{+}_{10}$ molecule features two covalent bonds between C_{70} and $C_{24}H_{10}$, and is thus much more stable than the singly bonded $C_{70}C_{24}H^{+}_{11}$ species. Additionally, there are clusters that correspond to $C_{70-}C_{24}H^{+}_{10-X}$ (where $X \leq 4$) at extremely low abundance.

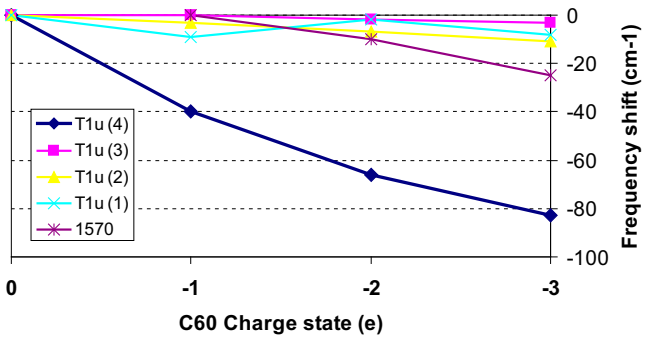

Fig. S8. Unscaled shifts in the four C_{60} IR-active modes (cm^{-1}) with charge state. Crosses indicate the calculated T_{1u} modes for Na@C_{60}, along with the new ~1,570 cm^{-1} with charge state corresponding to the calculated Mulliken charge transfer between the Na and the fullerene cage.

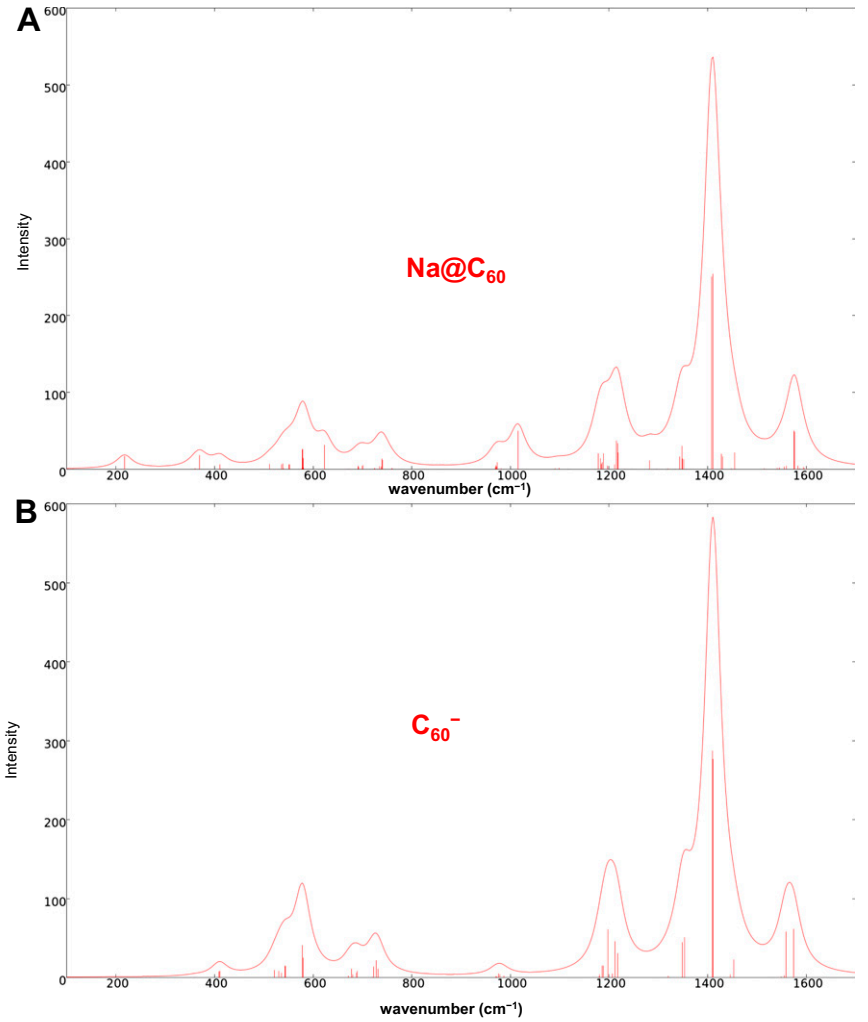

Fig. S9. Calculated unscaled FT-IR spectra with all IR-active frequencies marked by impulses. (*A*) Na@C_{60} and (*B*) C_{60}^-.

Table S1. Frequencies of the IR-active vibrational modes of C_{60} and Na@C_{60} from DFT calculations and experiment

			This work		
			C_{60}		Na@C_{60}
IR-active mode	Experiment (ref. 8)	Theory (ref. 7)	6-31G*	6-311G	6-311G
T_{1u} (1)	526	528	538	530 (525)	511 (506)
T_{1u} (2)	575	577	587	580 (574)	578 (572)
T_{1u} (3)	1,182	1,189	1,214	1,197 (1,185)	1,188 (1,176)
T_{1u} (4)	1,429	1,431	1,460	1,451 (1,436)	1,410 (1,396)

Frequencies from Bohnen et al. (7) include a 0.98 scaling factor. Following this approach, bracketed values include a 0.99 scaling factor.